Plasma Chem Plasma Process (2012) 32:427–450
DOI 10.1007/s11090-011-9339-7

ORIGINAL PAPER

Thermodynamics, Transport and Kinetics of Equilibrium and Non-Equilibrium Plasmas: A State-to-State Approach

M. Capitelli · I. Armenise · E. Bisceglie · D. Bruno · R. Celiberto · G. Colonna · G. D'Ammando · O. De Pascale · F. Esposito · C. Gorse · V. Laporta · A. Laricchiuta

Received: 22 July 2011 / Accepted: 2 December 2011 / Published online: 30 December 2011

Abstract Thermal non-equilibrium plasmas have been deeply investigated theoretically by means of the state-to-state approach, offering the unique opportunity of a detailed information about internal distributions affecting thermodynamics, transport coefficients and kinetics, properly accounting for the presence of excited states. The efforts made in the construction of knowledge on the dynamics of elementary processes occurring in the plasma with resolution on internal degrees of freedom, required by the method, are discussed. Boltzmann equation is solved for electrons self-consistently coupled to the chemical species collisional dynamics, reproducing very interesting features of strongly non-equilibrium internal distributions, characterizing plasmas.

Keywords Thermodynamics · Transport · Kinetic modeling · State-resolved cross sections

Introduction

Thermodynamics, transport and chemical kinetics of equilibrium and non-equilibrium plasmas is a topic of large interest, being the reproducibility of plasma technological products strongly dependent on our knowledge of the medium and of the relevant processes [1–3]. In this context, plasma modeling and diagnostics represent important issues to improve this knowledge. Usually plasma technology distinguishes between *thermal* and *cold* plasmas, the first characterized by local thermodynamic equilibrium (LTE) and the second by non-equilibrium between the different degrees of freedom, including the

M. Capitelli (✉) · G. D'Ammando · C. Gorse
Department of Chemistry, University of Bari, Bari, Italy
e-mail: mario.capitelli@ba.imip.cnr.it

M. Capitelli · I. Armenise · E. Bisceglie · D. Bruno · G. Colonna · G. D'Ammando · O. De Pascale · F. Esposito · C. Gorse · V. Laporta · A. Laricchiuta
IMIP CNR Bari, Bari, Italy

R. Celiberto
Department of Water Engineering and Chemistry, Polytechnic of Bari, Bari, Italy

chemical one. The characterization of these situations can be done using more or less sophisticated approaches, depending on the particular process under investigation, commonly based on statistical thermodynamics, kinetic theory and quantum chemistry. These aspects are particularly stressed when use is made of the so-called state-to-state approach that considers each excited state (rotational, vibrational and electronic) as an independent chemical species with its own thermal and kinetic properties. State-to-state models have been used in these years by our group to describe both thermal and non-thermal plasmas including thermodynamic and transport properties of equilibrium [4–10] and quasi-equilibrium plasmas [11–13], as well as kinetics in cold plasmas [14].

The state-to-state approach is peculiar in statistical thermodynamics [15] when complete sets (observed and missing) of energy levels are to be inserted in the electronic partition function subjected to a given cut-off criterion to avoid its divergence. In this case thousand and thousand energy levels must be considered even though recently an attempt to reduce the whole electronic manifold to a few (two or three) energy system is rather encouraging [16, 17].

More difficult is the state-to-state description of transport properties of thermal plasmas. This problem has been discussed by our group in numerous papers [18, 19] for the transport coefficients of an atomic hydrogen plasma formed by H(n), H^+ and electrons, where n is the principal quantum number of the excited atomic hydrogen. A complete set of transport cross sections has been derived for this system taking into account their dependence on the principal quantum number [18]. The global transport coefficients have been then calculated showing the role of excited states in affecting the corresponding quantities. The rigorous application of the Chapman–Enskog theory is able also to shed light on numerous compensation effects in the different terms, reducing the influence of excited states on the transport coefficients. Extension of these ideas to nitrogen and oxygen atomic plasmas is being considered by our group which in these last years has calculated resonant charge transfer [20–22, 54] and elastic [23] cross sections for the estimation of corresponding diffusion-type collision integrals involving low-lying and high-lying excited states. A preliminary attempt to estimate the role of excited states in affecting the reactive contribution to the thermal conductivity of a nitrogen plasma is reported in this paper.

The last part of our paper deals with the state-to-state kinetics of molecular plasmas. Plasma chemistry community knows the problem since the numerous contributions appeared in the literature on the subject mainly performed by Russian [24–26], Italian [14, 27−33] and Portuguese [34, 35] teams, reporting more or less complete models. The subject still suffers from the lack of complete sets of state-to-state cross sections and rates for the elementary processes acting in the different plasmas, a task in progress in our laboratory in the framework of FP7-Phys4Entry project [36]. In this paper we are focusing on the importance of complete sets of state-resolved dynamic data for up-pumping/deactivating processes of vibrational levels in the kinetics of N_2 by atom- and electron-impact collisions, i.e. on the role of the processes

$$N + N_2(v_i) \rightarrow N + N_2(v_f) \tag{1}$$

$$e + N_2(v_i) \rightarrow e + N_2(v_f) \tag{2}$$

in affecting the macroscopic properties of nitrogen plasmas, relying on accurate complete and consistent data sets recently obtained in the frame of quasi–classical trajectory (QCT) method [37, 38] and the local resonant theory [39], respectively.

In the last section some case studies are presented, discussing the differences arising in the vibrational and electron energy distributions by the inclusion of different data sets in the

kinetic model to emphasize the *completeness* issue. In particular, for the VTa process (1), being the parent-atoms considered as *killers* of vibrational energy through mono- and multi-quantum transitions, the relaxation of high temperature N_2 vibrational distribution in a low temperature bath is investigated. The results calculated using rates in references [37, 38] are compared with those obtained using older data set in references [40, 41], this last overestimating the rate coefficient for $T < 1{,}000$ K for the first vibrational levels ($\upsilon_i < \upsilon_f < 10$).

For the e-V processes (resonant vibrational excitation induced by electron impact) (2), discharge and post-discharge relaxation has been analyzed, evaluating the effects of using a reduced data set obtained collecting old results from references [42–45], limited to transitions with $\upsilon_f \leq 19$.

The examples do not end the list of the numerous elementary processes acting in the plasma. We refer in particular to the interaction of atomic species with the surface, a process which give vibrationally excited molecules i.e. atoms while destroying in gas phase the vibrationally excited molecules can reform them during the heterogeneous recombination [46, 47].

Thermodynamics and Transport Properties

The state-to-state approach applied to thermodynamics allows us to clarify the role of electronic states of atomic species in affecting important quantities such as frozen and reactive specific heats as well as isentropic coefficient [48]. On the other hand the dramatic dependence of transport cross sections of atom–atom, atom–ion interactions on the principal quantum number generates new perspectives in the understanding the transport properties of thermal plasmas [48]. We are aware of the difficulty to use the state-to-state approach in both thermodynamic and transport theories so that a strategy to simplify the relevant equations is in progress in our laboratory. This strategy implies the reduction of multi-level systems to few-level ones [15–17], which however contains the information (especially on the transport cross sections) about the thousands of electronic levels existing under thermal plasma conditions. Examples in this direction are reported for different high-temperature–high-pressure plasmas.

Three-Level Approach for Thermodynamic Properties of Atomic Nitrogen Plasma

The ground state configuration of atomic nitrogen is $^4S_{3/2}$ having statistical weight $g_1^\star = g(^4S) = 4$. There are other two low-lying levels resulting from $2s^2 2p^3$ electronic configuration, one corresponding to $^2D_{5/2,3/2}$ and one to $^2P_{3/2,1/2}$, whose energy and statistical weight are $g(^2D) = 10$, $\varepsilon(^2D) = 2.3838$ eV and $g(^2P) = 6$, $\varepsilon(^2P) = 3.5757$ eV, respectively. These two levels are grouped together to give a single low lying state which statistical weight, given by

$$g_2^\star = g(^2D) + g(^2P)$$

and characteristic temperature θ_2, calculated as

$$\theta_2 = \frac{g(^2D)\varepsilon(^2D) + g(^2P)\varepsilon(^2P)}{k\, g_2^\star}$$

are reported in Table 1.

Table 1 Degeneracy and characteristic temperature for atomic nitrogen considered as a three-level system, ground state, low lying level and upper lumped level, in *hydrogen-like approximation*, for different values of the maximum principal quantum number

	$g^{\star}$	θ (K)
Ground	4	0
Low-lying	16	32,849
n_{max}		
5	900	158,702
10	6,840	165,282
25	99,360	168,125
50	772,560	168,647
75	2,582,010	168,752
100	6,090,210	168,787

The energy of the other levels are calculated by using an *hydrogen-like approximation*

$$\varepsilon_n = I_{\mathrm{N}} - \frac{I_{\mathrm{H}}}{n^2} \tag{3}$$

(I_{N} and I_{H} are respectively the ionization potential of nitrogen and hydrogen atoms) and a statistical weight

$$g_n = 2n^2 g_{core} \tag{4}$$

[$g_{core} = 9$ represents the statistical weight of the ground state of the more stable nitrogen core (^3P)]. They are then grouped to form the third lumped level (see Table 1), limited to the maximum number n_{max}. A more accurate procedure to calculate the energies of electronically excited state consists in extending available (experimental or theoretical) data following the Ritz–Rydberg series [15].

In Fig. 1 we report the internal energy of atomic nitrogen considered as a three level system. Inspection of this figure shows that the internal energy of the atomic nitrogen strongly increases with the temperature as well as with the number of excited states considered in the internal energy. In both cases the internal energy is much higher than the translational one. Corresponding results for the internal specific heat for the same condition in Fig. 1 are reported in Fig. 2. The case of $n_{max} = 10$ shows a well defined maximum at

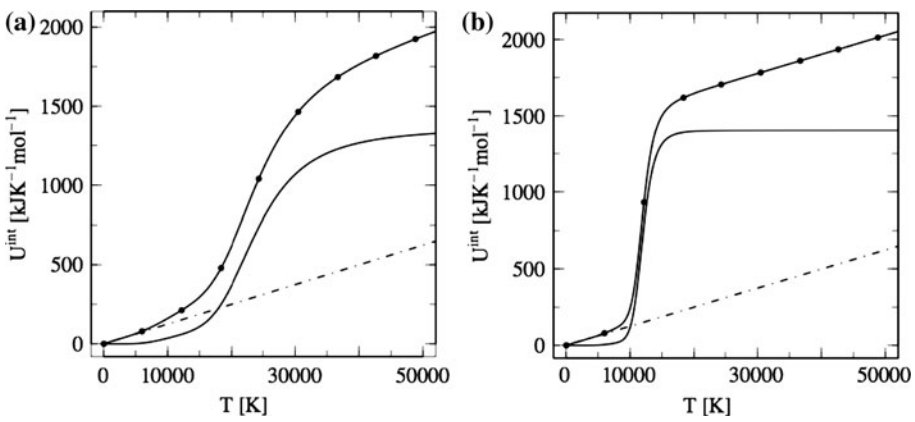

Fig. 1 Atomic nitrogen translational (*dashed-dotted line*), internal (*solid line*) and total (*closed markers*) molar energy as a function of the temperature for (**a**) $n_{max} = 10$ and (**b**) $n_{max} = 100$

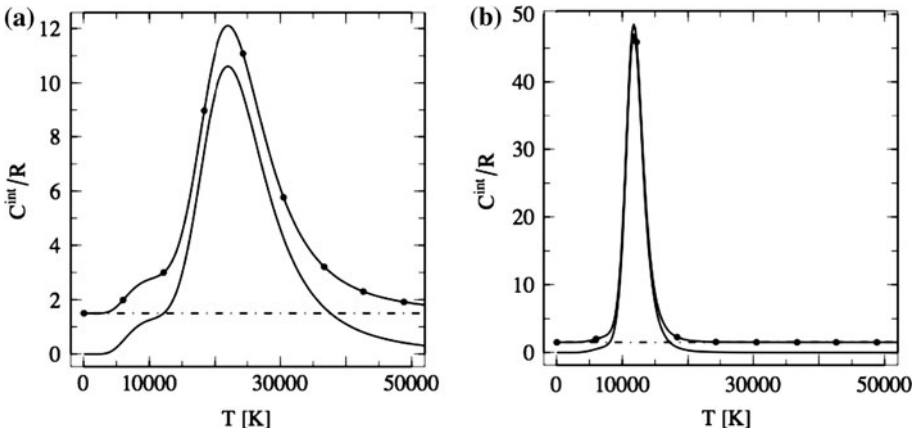

Fig. 2 Atomic nitrogen translational (*dashed-dotted line*), internal (*solid line*) and total (*closed markers*) reduced molar specific heat as a function of the temperature for (**a**) $n_{max} = 10$ and (**b**) $n_{max} = 100$

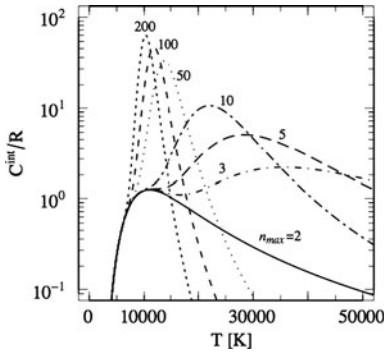

Fig. 3 Reduced internal specific heat of atomic nitrogen as a function of the temperature for different values of n_{max} (note that the case $n_{max} = 2$ considers only the low-lying states)

$T \approx 22{,}000$ K due to the high-lying excited levels with the onset of a secondary maximum at $T \approx 12{,}000$ K due to the low-lying excited states, that disappears in the $n_{max} = 100$ case. This point is evident in Fig. 3, where we report different $\bar{C}^{int}$ curves corresponding to different n_{max} values. In particular the curve labeled with $n_{max} = 2$ does not consider the third level: in this case the first maximum is well evident, disappearing as the degeneracy of the lumped level grows up.

The results reported in the different figures refer to atomic systems when the high-level energies are lumped allowing their dependence on the principal quantum number. They are in close agreement with the corresponding ones obtained by inserting complete set of levels subjected to the same value of n_{max} [16, 17].

Transport Coefficients with EES: Reactive Thermal Conductivity

The influence of electronically excited states (EES) on the transport properties of equilibrium atomic plasma has been investigated for hydrogen system. The ratio of the transport coefficients obtained neglecting, *usual* (*u*), and including, *abnormal* (*a*), the strong increase of transport cross sections with the principal quantum number of the excited hydrogen atoms, $H^{\star}(n)$ significantly departs from unity especially in high-pressure regimes [18, 49–53].

Moving to air plasmas demands the knowledge of a complete and consistent data-set of collision integrals for interactions involving excited states [20, 23, 54], a challenging issue far to be achieved. In this paper an attempt is shown to reduce the state-to-state to a *few-level approach* analogous to the thermodynamic one. The temperature profile of the reactive thermal conductivity is known to be governed by the binary diffusion coefficient for atom–ion interactions, this quantity being directly related to the diffusion-type collision integrals, $\sigma^2\Omega^{(1,1)\star} \equiv \Omega^{(1,1)}$, usually characterized by large values due to the dominant contribution of resonant charge-transfer processes in ion–parent-atom collisions.

The transport cross sections for $N^{\star} - N^{+}(^3P)$ interaction have been derived, in the frame of the asymptotic approach [55, 56], considering excited atomic partners, i.e. the low-lying states of nitrogen ($N(^2D,^2P)$) and high-energy states with electronic configuration characterized by an increasing value of the principal quantum number of the optical electron, $(^3P)_{core}ns$. In Fig. 4a corresponding diffusion-type collision integrals, for a fixed value of the temperature, are presented on a reduced energy scale ($n' = 2 - 1/n^2$), having also the advantage to represent the infinite limit for n on a finite scale. The state-selective results for the electronic terms $N(^2P,^4P)$ arising from the ns configuration are reported together with the thermal values. It should be stressed that in this averaging procedure over the sublevels characterized by the same principal quantum number, only few terms are included, assuming that other states contribute to the same extent, thus n-dependent collision integral values represent a low-limit estimate. The resonant process, mimicking an elastic collision leaving the quantum state of colliders unchanged, strongly affects the collision integrals that exhibit an increase with the principal quantum number with a power-law of the type n^5, that has been used as scaling relation for the extrapolation to higher n-values.

In the perspective of deriving a collision integral that, though not explicitly depending on n, retains the effect of existence of electronically excited states, a temperature-dependent average over the Boltzmann distribution has been performed

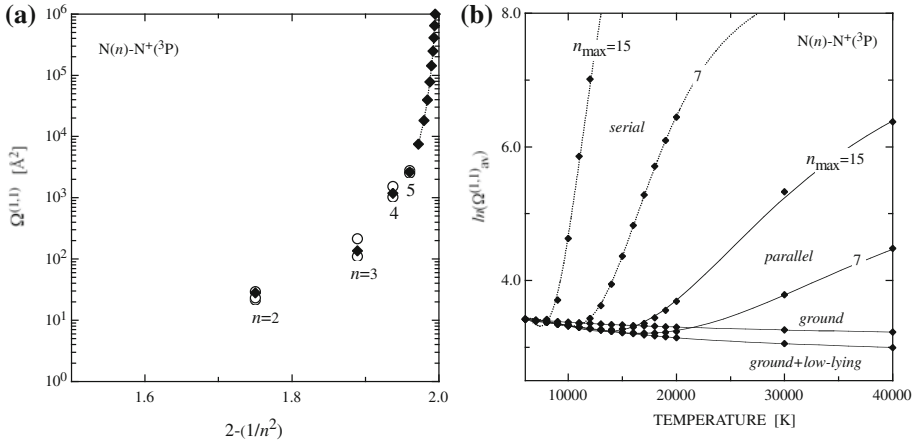

Fig. 4 (**a**) Dependence on principal quantum number (reduced energy scale) of inelastic contribution to diffusion-type collision integrals in $N^{\star} - N^{+}(^3P)$ interactions, at T=10,000 K. (*open markers*) state-selected values [20], (*closed markers*) average over sublevels with the same principal quantum number, (*dotted line*) extrapolation with n^5 scaling law. (**b**) Logarithmic value of the Boltzmann-average diffusion-type collision integral as a function of temperature for different number of terms included. *ground + low-lying* has been reported in the parallel approach

$$[\Omega_{av}^{(1,1)\star}]_{serial} = \frac{1}{\mathcal{Q}_{\mathrm{N}}^{int}}\Big[g(^4S)\Omega^{(1,1)\star}_{\mathrm{N}(^4\mathrm{S})-\mathrm{N}^+(^3\mathrm{P})} + g(^2D)\Omega^{(1,1)\star}_{\mathrm{N}(^2\mathrm{D})-\mathrm{N}^+(^3\mathrm{P})}e^{-\varepsilon(\mathrm{N}(^2\mathrm{D}))/kT} + g(^2P)\Omega^{(1,1)\star}_{\mathrm{N}(^2\mathrm{P})-\mathrm{N}^+(^3\mathrm{P})}e^{-\varepsilon(\mathrm{N}(^2\mathrm{P}))/kT} + \sum_{n=3}^{n_{max}} g_n^{\star}\Omega^{(1,1)\star}_{\mathrm{N}^{\star}-\mathrm{N}^+(^3\mathrm{P})}e^{-\varepsilon(\mathrm{N}^{\star})/kT}\Big] \quad (5)$$

where $\mathcal{Q}_{\mathrm{N}}^{int}$ is the internal partition function of atomic nitrogen, whose excited levels ($n > 3$) have been described in *hydrogen-like approximation*, thus estimating the energy and statistical weight of the ith level through (3) and (4). The terms up to a maximum value n_{max} have been included, selected on the base of a cut-off criterion compatible with the pressure in the system. This average has been labelled as *serial* with respect to a *parallel* scheme in which the value results from the average

$$[(\Omega_{av}^{(1,1)\star})^{-1}]_{parallel} = \frac{1}{\mathcal{Q}_{\mathrm{N}}^{int}}\Big[g(^4S)(\Omega^{(1,1)\star}_{\mathrm{N}(^4\mathrm{S})-\mathrm{N}^+(^3\mathrm{P})})^{-1} + g(^2D)(\Omega^{(1,1)\star}_{\mathrm{N}(^2\mathrm{D})-\mathrm{N}^+(^3\mathrm{P})})^{-1}e^{-\varepsilon(\mathrm{N}(^2\mathrm{D}))/kT} + g(^2P)(\Omega^{(1,1)\star}_{\mathrm{N}(^2\mathrm{P})-\mathrm{N}^+(^3\mathrm{P})})^{-1}e^{-\varepsilon(\mathrm{N}(^2\mathrm{P}))/kT} + \sum_{n=3}^{n_{max}} g_n^{\star}(\Omega^{(1,1)\star}_{\mathrm{N}^{\star}-\mathrm{N}^+(^3\mathrm{P})})^{-1}e^{-\varepsilon(\mathrm{N}^{\star})/kT}\Big] \quad (6)$$

In fact, in complete analogy with an electrical circuit, the transport phenomena in plasma could be thought as hindered by collisions and the electronically excited states act as resistors characterized by higher resistance thus influencing the global value. The two schemes corresponds to a serial-resistor and parallel-resistor circuits. Average values of diffusion-type collision integral have been displayed in Fig. 4b for different choices of n_{max} ($n_{max} = 15$ and 7 for $p = 1$ and 100 atm, respectively), including also the *ground* case and summation extended only to the electronic terms for the valence shell ($n = 2$). It should be noted that the *low-lying* excited states actually reduce the $\Omega_{av}^{(1,1)\star}$ value affecting the global collision integral in the temperature range [10,000–20,000 K] even when the high-lying excites states are considered.

The reactive thermal conductivity, λ_r, calculated within the first-order Chapman–Enskog approximation and in the ground state approximation for all other relevant

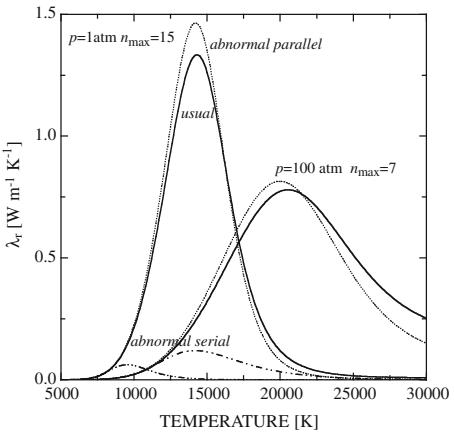

Fig. 5 Reactive thermal conductivity as a function of temperature for different pressures and schemes

interactions, has been reported in Fig. 5, for the two selected pressures, as resulting from the different schemes. The *serial-scheme* seems to overestimate the EES role, producing a strong compression of the transport as already observed in reference [51] for the average multi-component diffusion coefficient. On the contrary, the *parallel-scheme*, corresponding to a physical picture in which the transport proceeds through the channel with minor resistance, gives results in closer agreement to what obtained in the rigorous state-to-state approach applied to the atomic hydrogen plasma [51]. The relevant role of low-lying excited states, always significantly populated in the considered temperature window, determines the higher values of λ_r in the region of the peak, while for further temperature increase the highly-excited states reduce this value, leading to a λ_r^a/λ_r^u ratio lower than 1.

Kinetics

Non-equilibrium plasma kinetics is the other topic for which the state-to-state approach becomes important and in some cases essential. A considerable progress has been achieved in the literature since the first appearance of self-consistent state-to-state models, presented by different international groups, for N_2 and H_2 plasmas. In these approaches the state-to-state kinetics was coupled with a Boltzmann solver for the electron energy distribution function (eedf), the mutual interaction being mainly driven by second-kind collisions involving electronically and vibrationally excited molecules [57].

These kinetic models are nowadays also inserted either in PIC (particle in cell) [58, 59] models or in fluid dynamic codes [60–63]. The difficulty of the state-to-state approach in non-equilibrium plasma kinetics is mainly represented by the still poor knowledge of the collision cross sections for the different inelastic channels [27, 64]. The situation is however rapidly progressing for molecular plasmas involving N_2, O_2 and H_2, especially concerning the vibrationally-resolved cross sections and rates for electron-molecule and atom-molecule processes. On the other hand. molecular dynamics calculations give evidence of the remarkable production of vibrationally excited molecules during the recombination of atoms on the plasma reactor surface, this process having, at high pressure, large similarities with the three-body gas-phase atomic recombination. In this context it is of great relevance the theoretical investigation on heterogeneous processes, leading to different exit channels, including atomic recombination and molecular vibrational deactivation.

The difficulties in the implementation of state-to-state models are however compensated by the detailed information provided about the non-equilibrium rotational, vibrational and electronic distributions existing in the plasma, as well as the non-Maxwell character of the eedf. These distributions, which are not easily accessible by dedicated experiments, play an important role in determining macroscopic properties of the plasma including dissociation and ionization degrees.

Dynamics of Elementary Processes

Resonant Vibrational Excitation in e-N_2 Collisions

The resonant vibrational excitation of nitrogen molecules by low-energy electron impact is a process that efficiently promote the vibrational pumping mechanism and, in the interplay with vibration–translation and vibration–vibration energy transfer in heavy particle collisions and dissociation/recombination dynamics, determines the profile of the N_2

vibrational distribution function. The channel involving the temporary formation of the negative molecular ion in its ground electronic state (2.3 eV shape resonance),

$$N_2(^1\Sigma_g^+, v_i) + e \rightarrow N_2^-(^2\Pi_g) \rightarrow N_2(^1\Sigma_g^+, v_f) + e \quad (7)$$

has been investigated since many years both experimentally [65–67] and theoretically [68–72], in the frame of different approaches. Recently [39] new calculations have been performed within the *local theory of resonance* [73] for the derivation of a complete set of cross sections, i.e. mono- and multi-quantum vibrational excitations among the 67 levels in the vibrational ladder of the ground state for N_2 molecule, resulting in a huge number of transitions. The energy dependence of the cross section exhibits, as already observed, oscillatory features due to the interference with the vibrational manifold of the molecular ion.

In Fig. 6a the mono-quantum excitations are displayed for selected values of the initial vibrational quantum number. As expected, increasing v_i produces a lowering of the process threshold, the cross section energy-profile being characterized by a broadening of the region presenting oscillations with narrow peaks of reduced absolute value. The multi-quantum excitations, in Fig. 6b, are as a rule less favored than mono-quantum ones with thresholds shifted to the high-energy region. Also in this case considering higher terms in each series, i.e. characterized by higher initial vibrational level, an extension of the cross section peak-structure both in the low- and high-energy regions is observed, with evidence of increasing peak height for high Δv. A general agreement is found with theoretical results available in literature [68], both in position and amplitude of cross section peaks. Good agreement is observed with the experimental measurements of Allan [44] and Wong [68] as shown in Fig. 6.

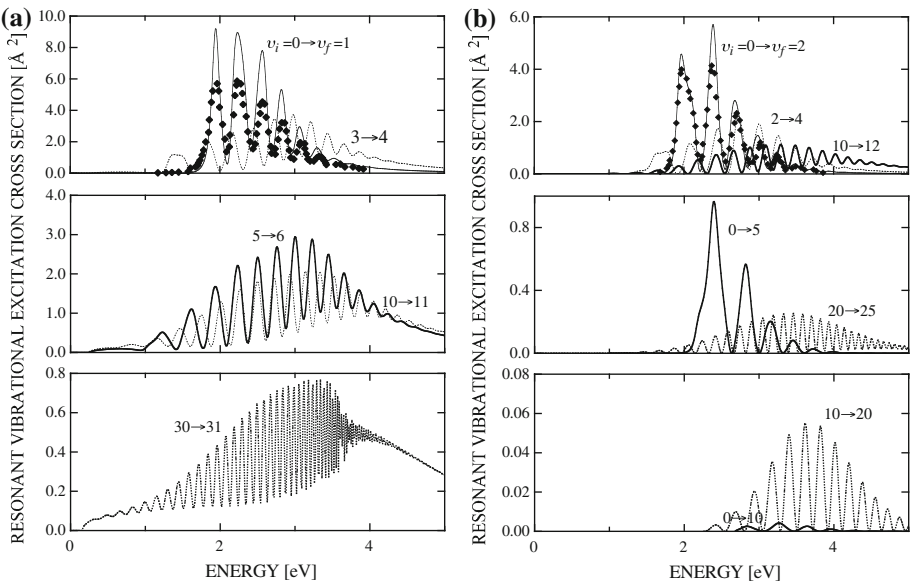

Fig. 6 Resonant vibrational excitation cross sections as function of collision energy for selected (**a**) mono-quantum $v_i \rightarrow v_f = v_i + 1$ and (**b**) multi-quantum $v_i \rightarrow v_f = v_i + 2$ or $v_i + 5$ or $v_i + 10$ excitation transitions (*closed markers*) experimental results [68] for 0→1 and 0→2 excitations

Integration over a Maxwellian electron energy distribution function (eedf), leads to corresponding state-resolved rate coefficients for thermal equilibrium case.

These rates can be confidently used in aerospace applications, where the electron density is high enough to thermalize the eedf. Under non-equilibrium conditions the rates for e-V processes shall be derived by integration over a distribution function obtained by the solution of the Boltzmann equation [74], accounting also for the presence of excited states, as done in Sect. 3.3. The importance of using a non-Maxwell eedf has been pointed out in Refs. [75, 76], where the large differences occurring, especially for high-threshold processes, are discussed. In any case the rates reported in this section are of interest for understanding the dependence of elementary processes on the vibrational quantum number.

Figure 7 shows the rate coefficients calculated for the transitions $\upsilon_i = 0$ to υ_f ranging from 0 to 5 as a function of the electron temperature, successfully compared with the calculations of Huo et al. [42]. The mono-quantum excitation rates, displayed in Fig. 8a, show two different dependencies on the initial vibrational level in the low- and medium-high-temperature regions. In fact, above $T \approx 0.4$ eV the rates are monotonically lowered increasing υ_i, while below 0.4 eV the behavior is characterized by a maximum around $\upsilon_i = 10$. The threshold effect, usually responsible of the low-temperature increase of the rate with the vibrational level, in this case seems inefficient, except for the first transitions, while dominated by the extension of the area under the resonance spectra. This bimodal character of the vibrational profile was also observed in reference [77], where the analysis was limited to few transitions up to $\upsilon_i = 12 \rightarrow \upsilon_f = 13$, finding in general a satisfactory agreement, though the new calculation predicts higher values. In Fig. 8b the vibrational profiles of rates for mono- and multi-quantum excitation at fixed temperature are shown. Increasing the number of vibrational quanta the rate is strongly decreased, according to the corresponding cross section behavior, but more interesting is the different role of vibrational excitation of the target that acts by reducing the resonant process probability for low $\Delta\upsilon$ values, while producing a significant enhancement for $\Delta\upsilon > 10$, with bimodal profiles in the transition between the two regimes.

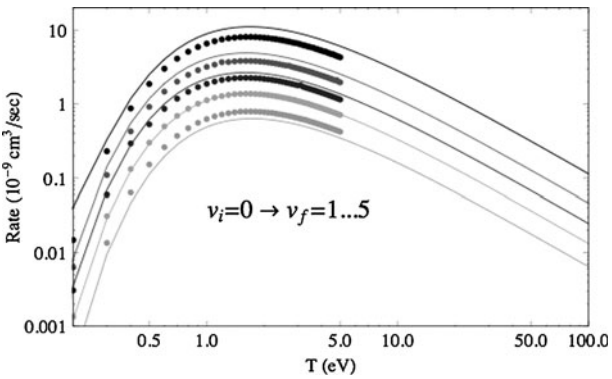

Fig. 7 Resonant vibrational excitation rate coefficients as function of electron temperature for selected excitations $\upsilon_i = 0 \rightarrow \upsilon_f = 1, \ldots, 50$ (*solid lines*) new results [39], (*closed markers*) results by Huo et al. [42]

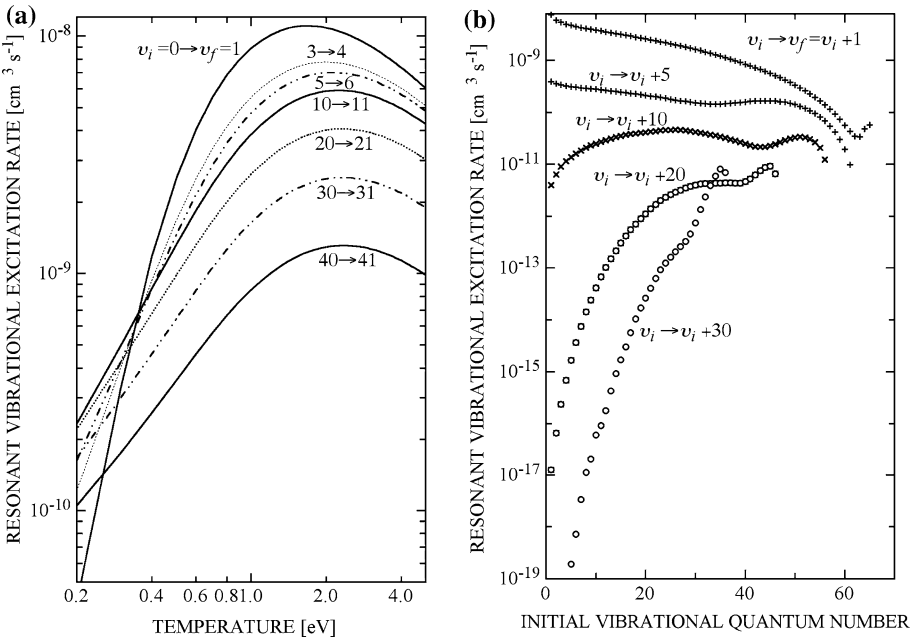

Fig. 8 Resonant vibrational excitation rate coefficients (**a**) as function of electron temperature for selected mono-quantum $\upsilon_i \rightarrow \upsilon_f = \upsilon_i + 1$ and (**b**) as a function of initial vibrational quantum number for multi-quantum $\upsilon_i \rightarrow \upsilon_f = \upsilon_i + n$ excitation transitions for electron temperature $T = 1$ eV

VT and Dissociation in N–N_2 Collisions

The accurate determination of vibrational detailed rate coefficients of heavy particle collision processes is nowadays considered an important issue to solve for a reliable theoretical treatment of plasma processes. However, often in the literature approximate general models are present to cope with this problem, considering just the non-reactive and often totally ignoring reactive collisions. A contribution to the accurate determination of rates for the process (1), which is of large importance for mixtures containing air, was given by Armenise et al. [41], with the publication of interpolated rates based on quasiclassical calculations of Laganà et al. [40], on the potential energy surface of the same authors, and including both reactive and non-reactive transitions (see also [78–81]), rates widely used in plasma chemistry [82, 83]. However, the original data in reference [40] do not include extremes of vibrational axis, limiting υ_i to the interval 5–45. Recently, very detailed and accurate quasiclassical (QCT) cross section calculations have been performed by Esposito et al. [37], including a complete rate interpolation of the whole vibrational ladder [38]. In reference [84] dissociation from vibrational excited molecules has been calculated.

In Fig. 9a and b a comparison of QCT rates [37, 38] with interpolated rates [41], properly rescaled in order to cover the whole vibrational ladder, at $T = 500$ and 1,000 K, is displayed. It is worth to note that the old interpolation could be considered as an acceptable approximation for higher vibrational levels, but the low-υ extrapolation ($\upsilon < 10$) is quite inaccurate at the considered temperature values.

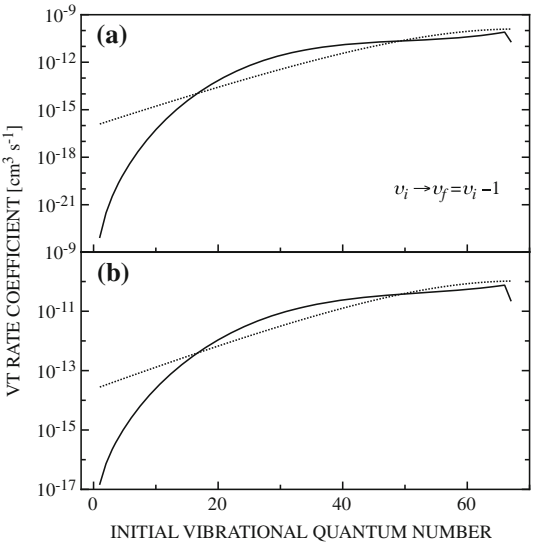

Fig. 9 Mono-quantum vibrational de-excitation rate coefficients as a function of initial vibrational quantum number, at $T = 500$ K (**a**) and $T = 1{,}000$ K (**b**). (*Dotted line*) [41], (*solid line*) [38]

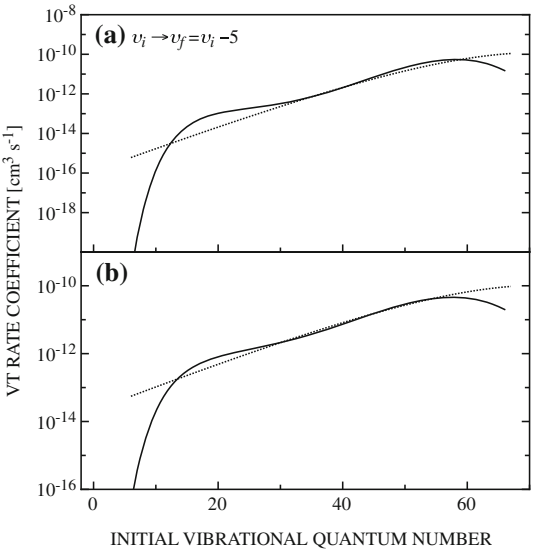

Fig. 10 Multi-quantum ($\Delta\upsilon = 5$) vibrational de-excitation rate coefficients as a function of initial vibrational quantum number, at $T = 500$ K (**a**) and $T = 1{,}000$ K (**b**). (*Dotted line*) [41], (*solid line*) [38]

For multi-quantum vibrational de-excitation processes, essentially the same observations done for mono-quantum case applies, as it can be appreciated by inspection of Fig. 10a and b, where the two series of results for the $\Delta\upsilon = 5$ are displayed.

Finally *VT* rates in reference [40] originated also dissociation in the frame of the *ladder climbing* (LC) model [41]. Figure 11 clearly shows a considerable discrepancy between LC and QCT dissociation rates, the ladder climbing model underestimating dissociation by approximately two orders of magnitude at $T = 500$ and 1,000 K, leading to the general conclusion that it should be regarded as a very rough approximation of dissociation, at least in the case of atom–diatom collisions.

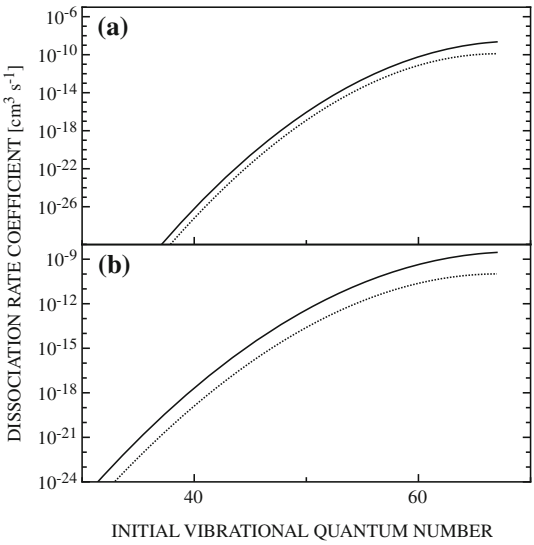

Fig. 11 Dissociation rate coefficients as a function of initial vibrational quantum number, at $T = 500$ K (**a**) and $T = 1{,}000$ K (**b**). (*Dotted line*)—ladder climbing model [41], (*solid line*)—QCT results [38]

Formation of Excited N_2 Molecules in Heterogeneous Processes

Though not included in the kinetic model here presented, it must be mentioned the significant role played by the heterogeneous deactivation/recombination dynamics at the surface in the onset of non-equilibrium distributions of ro-vibrational and electronic levels of molecules. These processes are modeled through two relevant mechanisms, i.e. the *Eley–Rideal recombination* of one atom physi- or chemisorbed at one site of the surface interacting with one atom in the gas phase, characterized by kinetic energy and angular orientation, and the *Langmuir–Hinshelwood recombination* of two physisorbed atoms.

The recombination probability of atomic nitrogen at the silica surface (β-cristobalite crystalline structure), assisted by the phonon excitation of the crystal substrate, has been investigated, in the frame of a semi-classical approach for the Eley–Rideal collisional mechanism, at $T = 1{,}000$ K [47]. Theoretical probability is characterized by a narrow peak, localized at collision energy of the impinging on the surface $E_{kin} = 0.055$ eV , while increasing the energy the recombination mechanism becomes largely inefficient, due to a favored trapping of atoms at the surface.

The nascent vibrational profile of N_2 molecules, corresponding to the maximum, is reported in Fig. 12, showing the highest probability of formation in the vibrational level $\upsilon = 0$, with a second broad maximum around $\upsilon = 25$, affecting the tail of the vibrational distribution. The rotational excitation is found to be ineffective in the whole impact-energy range.

Hypothesis of different heterogeneous mechanisms have been formulated, leading to the formation of electronically excited states of $N_2^{\star}$, i.e. $A^3\Sigma_u^+$ metastable state which plays an important role in the nitrogen afterglow [57, 85, 86].

Nitrogen State-To-State Kinetics

Relaxation of N_2 Vibrational Distribution in the Presence of N Atoms

As a first example we follow the relaxation of the vibrational distribution of N_2 in the presence of different concentrations of nitrogen atoms. The initial distribution is a

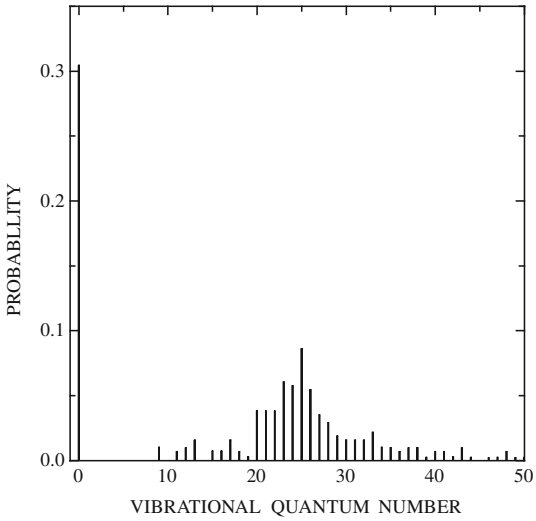

Fig. 12 Vibrational population distribution of N_2 molecules formed by atomic recombination on a silica surface at temperature $T_S = 1{,}000$ K and kinetic energy $E_{kin} = 0.055$ eV [47]

Boltzmann one at $T = 7{,}000$ K, $p = 2$ torr, subjected to an instantaneous decrease of the gas temperature to $T = 500$ K. The aim of this case is to stress the importance of using complete and accurate data sets for VT mono- and multi-quantum transitions as those reported in Figs. 9 and 10, as well as for recombination rates obtained from dissociation (Fig. 11) through detailed balance principle. The impact of atom-molecule deactivation rates, VTa, acting on the initial vibrational distribution function has been investigated by considering three groups of processes

(1) only VTa
(2) VTa plus the relaxation by molecules, i.e. VTm [87] and VV [88–90] (vibration–vibration) energy exchange processes
(3) VTa, VTm, VV plus dissociation–recombination processes

Two cases have been considered differing in the fraction of nitrogen atoms (35 and 1%). To better understand the results we want to remind that in any case the relaxation should end to a Boltzmann distribution at $T = 500$ K and that the rates acting in the relaxing system are calculated at this temperature. During the relaxation, the interplay between VV and VT rates could form a plateau in the vibrational distribution function whose extension depends on the relative magnitude of VT and VV rates. On the other hand, in case (3), the distribution function of vibrational levels near the continuum are dominated by the recombination in synergy with VT rates, which tend to thermalize the distribution. These ideas report the reader to many years ago when this kind of effects have been largely discussed [74, 91].

Let us first consider the relaxation of the initial Boltzmann distribution in the presence of the larger concentration of atoms. The results are reported in Fig. 13 a_i–b_i, corresponding to the conditions (1)–(3), i.e. to the progressive insertion of the different processes. The results in (a_i) figures have been obtained by atom–molecule VT and dissociation rates reported in ref. [38] (hereafter called VTaE and DisE), while the (b_i) figures correspond to the VT rates of Laganà as fitted by Armenise et al. in reference [41] and by the ladder climbing model, i.e. by extrapolating the multi-quantum transitions to the continuum, (hereafter called VTaA and DisA). Note that VTaE are orders of magnitude

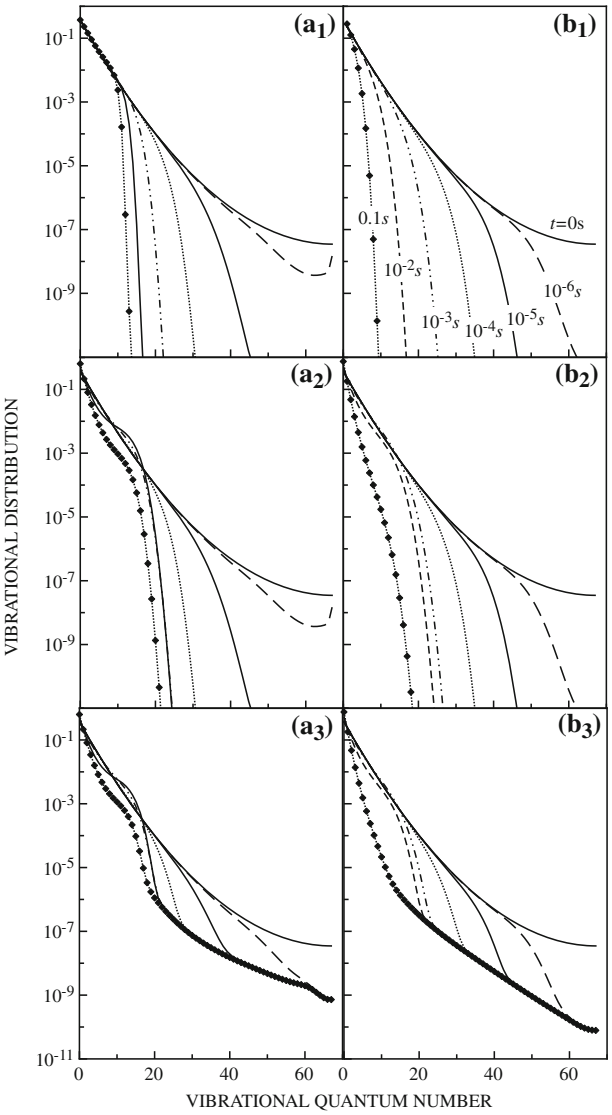

Fig. 13 Vibrational population distribution of N_2 ground state for different time-shots in the relaxation for initial atomic nitrogen molar fraction $\chi_N = 0.35$, for different conditions [cases (1)–(3)]. (**a$_i$**) rates of reference [38], (**b$_i$**) rates of reference [41]

lower than the corresponding VTaA for $\upsilon < 10$, while DisE rates are much higher than the corresponding DisA rates, this last behavior reflecting in the corresponding recombination rates. As a result we should obtain a lower relaxation of the first 10 levels of nitrogen when use is made of Esposito et al. rates and a more pronounced recombination plateau in the case (3). These qualitative considerations are recovered in the results reported in the different figures where the lower VTaE are not able to relax the vibrational distribution for $\upsilon < 10$ compared with the use of VTaA rates. Note also that the presence of VV rates with

the VTaE rates are such to create a shoulder in the distribution function that is absent when use is made of VTaA rates.

Finally the recombination rates from the accurate QCT dissociation by Esposito et al. are able to create a second declining plateau in the vibrational distribution function not present when use is made of the ladder climbing model. In this case the concentration of atoms is high enough to quench the plateau for $\upsilon > 10$. The behavior drastically changes when we limit the presence of atomic nitrogen to 1% (Fig. 14). In this case the VTa processes affect the distribution only for $\upsilon > 30$ while VV up pumping mechanism is able to create a declining plateau from $\upsilon = 5$ to $\upsilon = 30$ ($t = 10^{-2}$ s) and from $\upsilon = 5$ to $\upsilon = 20$ ($t = 0.1$ s). In any case VTaE and VTaA for $\upsilon > 15$ produce the same relaxation. Similar

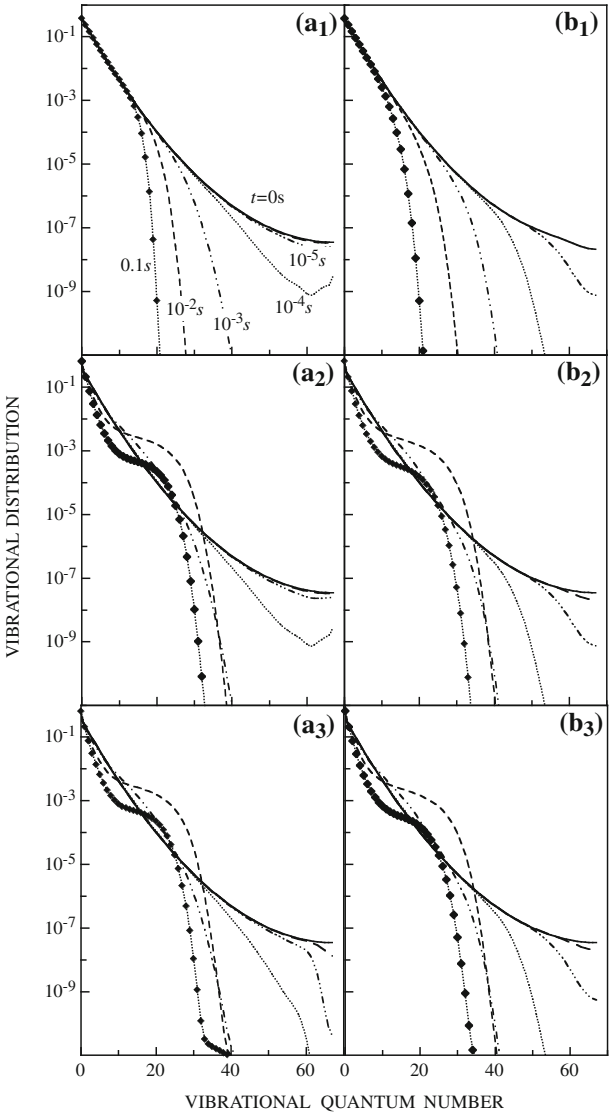

Fig. 14 Vibrational population distribution of N_2 ground state for different time-shots in the relaxation for initial atomic nitrogen molar fraction $\chi_N = 0.01$, for different conditions [cases (1)–(3)]. ($\mathbf{a_i}$) rates of reference [38], ($\mathbf{b_i}$) rates of reference [41]

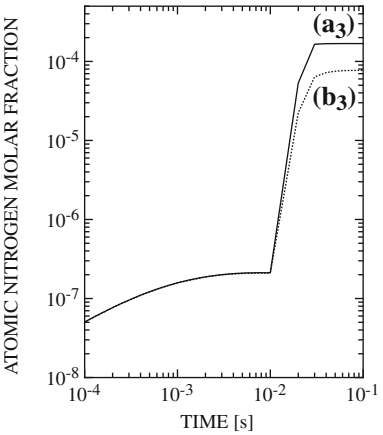

Fig. 15 Atomic nitrogen molar fraction as a function of time for case (3). (a_3) Rates of reference [38], (b_3) rates of reference [41]

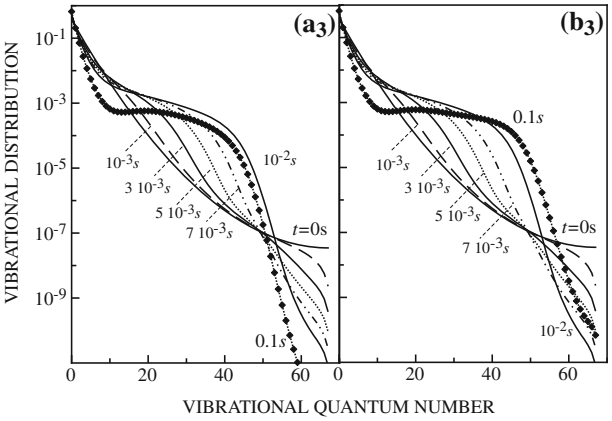

Fig. 16 Vibrational population distribution of N_2 ground state for different time-shots in the relaxation for initially absent atomic nitrogen ($\chi_N = 0.0$), for case (3). ($\mathbf{a_i}$) Rates of reference [38], ($\mathbf{b_i}$) rates of reference [41]

results are also observed when recombination process is included, being its contribution negligible at such atomic concentration.

The results presented in the previous figures show that the deactivation of high lying vibrational levels by atom–diatom collisions is important also for small fractions of atomic nitrogen, i.e. $\chi_N = 0.01$.

We can examine a new condition where, starting from $\chi_N = 0$, the atoms can be formed during the relaxation from vibrationally excited molecules considering processes in case (3). Figure 15 reports the concentration of atomic nitrogen calculated with the two sets of VTa and Dis rates. Independently of the used data set, the concentration of atomic nitrogen remains small, being in the case of Esposito data 2 times larger than the Laganà ones. It is worth noticing that, during the relaxation of the vibrational distribution of N_2, reported in Fig. 16a and b, a long plateau is observed due to the presence of VV processes, balanced by VTm when atomic nitrogen concentration is low.

Nanosecond Discharge

To establish the importance of new complete set of e-V cross sections, we run a numerical experiment where a reduced electric field of 100 Td is applied to an atmospheric nitrogen system for 10 ns followed by a post-discharge of 100 μs. We compare the results obtained with the complete set of e-V cross sections (hereafter called eVL) and with a set of cross sections used in these years by our group (hereafter called eVC). These last use the experimental e-V cross sections by Allan [44] ($\upsilon_i = 0 \rightarrow \upsilon_f = 1 - 17$) completed by the theoretical data by Morgan [43] ($\upsilon_i = 0 \rightarrow \upsilon_f = 18, 19$) and the e-V cross sections by Chandra and Temkin [45] ($\upsilon_i = 1 - 7 \rightarrow \upsilon_f = \upsilon_i + 1 - 8$). The numerous other elementary process rates are the same when using eVL and eVC. Figure 17 reports the molar fractions of electrons, $N_2(A^3\Sigma_u^+)$ metastable state and atomic nitrogen calculated with the two data sets for e-V processes. The differences in concentrations, even if small, are able to affect eedf in the post-discharge condition (see Fig. 18).

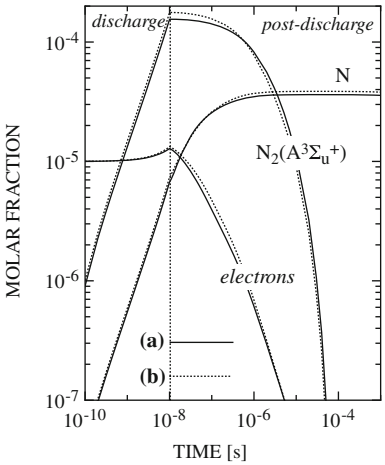

Fig. 17 Atomic nitrogen molar fraction as a function of time. (*a*) eVL [39], (*b*) eVC [43, 44, 45]

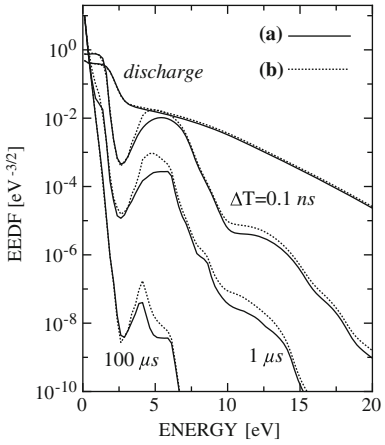

Fig. 18 Electron energy distribution function for different time-shots in the discharge and post-discharge phases. (*a*) eVL [39], (*b*) eVC [43, 44, 45]

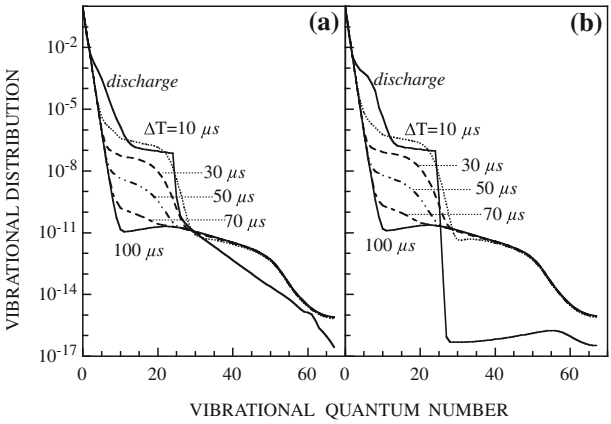

Fig. 19 Vibrational population distribution of N_2 ground state for different time-shots in the discharge and post-discharge phases. (**a**) eVL [39], (**b**) eVC [43, 44, 45]

In particular, the height of peaks, due to the *second-kind collisions* involving cold electrons and $N_2(A^3\Sigma_u^+)$, depends on the selected cross section set, showing higher values for eVC data. This behavior is a consequence of the limited number of e-V transitions considered in eVC set ($\upsilon \leq 19$), thus reducing the energy lost by electrons in vibrational excitation, as it can be appreciated in Fig. 19a and b displaying the temporal evolution of vibrational distribution. However, in both discharge and post-discharge phases, heating of the vibrational distribution is not observed. This situation on the other hand reinforces the role of second-kind collisions from electronically excited states in affecting eedf in the post-discharge [92, 93].

It should be noted that the eedf reported in Fig. 18 could generate a negative absolute mobility [94–96].

Continuous N_2 Discharge

The last example we want to examine concerns the coupling between the different kinetics and the eedf in a continuous discharge. In this case we imagine a N_2 discharge submitted to an *E/N* value of 60 Td running at a pressure of 5 torr and $T_g = 1{,}000$ K. The initial situation is characterized by a Maxwell distribution function at $T_e = 1{,}000$ K and a corresponding vibrational temperature of $T_\upsilon = 1{,}000$ K. The initial molar fraction of electrons is considered to be 10^{-5}. For $t > 0$ all distributions start to be excited generating a strong coupling between eedf and vibrational and electronic distributions as can be seen from Fig. 20, where the distribution time evolution has been reported. Moreover in Fig. 21 we report the concentration of electrons, of metastable $A^3\Sigma_u^+$ state and of nitrogen atoms. It should be noted that, at the stationary condition, the 0–1 vibrational temperature reaches a value of 12,000 K. We note the strong dependence of low energy eedf on the vibrational temperature as well as the strong dependence of high energy eedf on the concentration of electronic states. This behavior is due to the action of second-kind vibrational and electronic collisions. Looking at Fig. 20b we can see a well developed vibrational distribution even though we note the lack of plateau regimes. This well developed vibrational distribution is able to increase the macroscopic dissociation and ionization rates. As an example in Fig. 22 we report the dissociation rate of N_2 by electron impact as a function of time by considering the dissociation from $\upsilon = 0$, the dissociation from $\upsilon > 0$ and the *total* dissociation rate. The dependence of the dissociation cross sections on the vibrational quantum

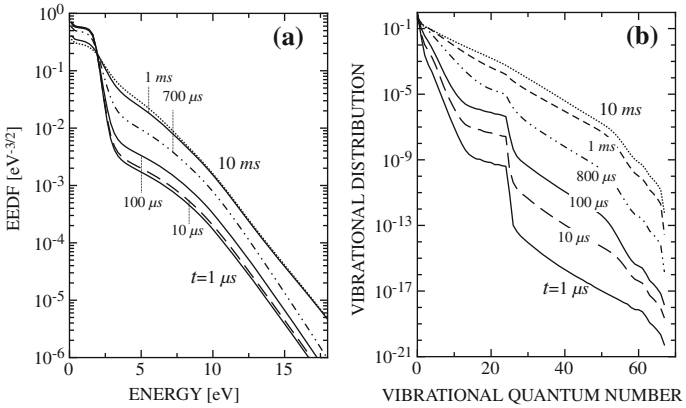

Fig. 20 Vibrational population distribution of N_2 ground state for different time-shots in the discharge phase. (**a**) eVL [39], (**b**) eVC [43, 44, 45]

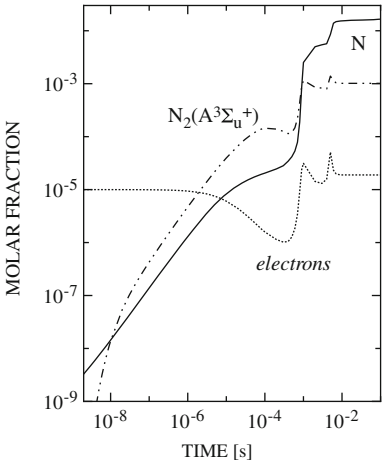

Fig. 21 Molar fractions of electrons, nitrogen atom and metastable electronic state of N_2, as a function of time during continuous discharge

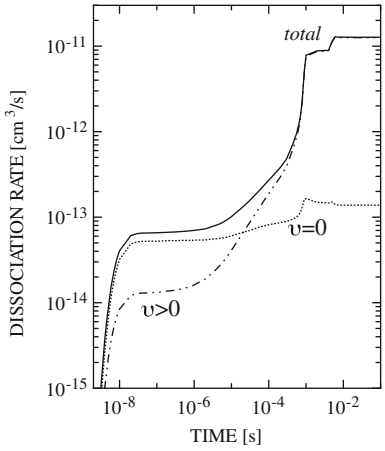

Fig. 22 Electron-impact dissociation rates as a function of time. Contribution of the vibrational level $\upsilon = 0$, of all vibrational excited levels, $\upsilon > 0$, and resulting *total* dissociation rate

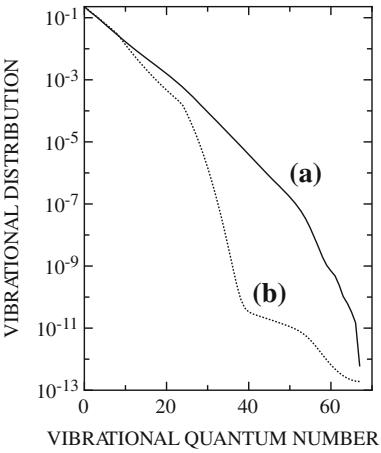

Fig. 23 Vibrational population distribution of N_2 ground state at $t = 0.1$s. (*a*) eVL [39], (*b*) eVC [43, 44, 45]

number has been reported in reference [97]. Inspection of Fig. 22 shows the strong increase of the macroscopic dissociation rate coming from vibrationally excited molecules, a process which can not be disregarded in nitrogen discharges. A better clarification of this point needs a further effort in the calculation of a complete set dissociation cross section taking into account their vibrational dependence being beyond our calculated cross sections. Another point which deserves further attention is the role of pure vibrational mechanisms in the dissociation process. Under this case study, this contribution is very small due to the large VTa rates, involving high-lying vibrational levels, which do not allow the formation of the plateau in the vibrational distribution. This point must be taken into consideration when dealing with plasmas running at very low temperature, i.e when VTa loose their importance.

We can also appreciate the importance of having a complete set of e-V cross sections comparing the results obtained with the data in reference [39] and those in references [43–45] as in the previous section (see Fig. 23). The high-energy levels are populated mainly by e-V processes between vibrationally excited states, in a sort of ladder climbing model. These processes are limited to few transitions ($\upsilon_f \leq 8$) in case (*b*) while in case (*a*) the whole matrix of transitions is considered. We should point out that the two models differ only by the set of e-V cross sections, using the same data for all the other processes. On the other hand, the eedf's in the discharge are very similar in the two cases, because, in the presence of high field, the balance between inelastic and second-kind collisions mitigate the differences between the data sets. The rates of electron impact dissociation are weakly affected by e-V processes, in spite of the differences in the vibrational distributions, because only levels with $\upsilon_f \leq 20$ contribute effectively to the dissociation process.

Conclusions

The presented results can be considered indicative of the importance of a state-to-state approach in improving our knowledge of thermal and cold plasmas. Concerning thermal plasmas we can say that the two- or three-level models can be used with a fair amount of confidence in the calculation of the partition function of monoatomic species allowing an actual consideration of excited states in this important quantity. Concerning the transport properties of thermal plasmas the state-to-state approach is still at its infancy for atomic

plasmas with the exception of hydrogen. The attempt presented in this paper to modify the diffusion type $N–N^+$ transport cross sections, weighting in a *parallel* way the transport cross sections of excited states, seems promising. This method should be extended to other quantities such as viscosity and translational thermal conductivity.

The state-to-state plasma kinetics is passing from a qualitative understanding to a quantitative predictive tool especially for molecular H_2, N_2, O_2 plasmas and their mixtures. The efforts made by our group in the development of cross sections and rates depending not only on the energy but also on the quantum numbers of the target will permit to increase the reliability of the state-to-state approach in the description of plasma reactors to be used in different technological applications.

In the next future electron-molecule cross sections depending on the vibrational quantum number should reach the same accuracy of the corresponding data for electron-ground state molecule derived from deconvolution of transport coefficients [98].

In addition to the reported cases a similar effort is being made on $O–O_2$, $H–H_2$, $H^+–H_2$, $O–N_2$, $N–O_2$, systems as well as on $e–O_2(\upsilon)$, $e–NO(\upsilon)$ ones. Particular attention is devoted to the PES governing the atom–diatom interactions. It is worth noting that very recently appeared in the literature two new PES for $N–N_2$ system [99–101], which could change the rates published in this paper. Apparently however the use of these new PES should decrease the magnitude of VTa rates thus decreasing the role of atomic nitrogen in relaxing the vibrational distribution.

In conclusion state-to-state plasma kinetics while confirming the early results based on incomplete sets of cross sections can give further impulse to the development of new mechanisms for future applications.

Acknowledgments The research leading to these results has received funding from the European Community's Seventh Framework Programme (FP7/2007-2013) Under Grant Agreement No. 242311.

References

1. Boulos MI, Fauchais P, Pfender E (1994) Thermal plasmas: fundamentals and applications, vol 1. Plenum Press, New York
2. Fridman AA (2008) Plasma chemistry. Cambridge University Press, Cambridge
3. Capitelli M, Ferreira CM, Gordiets BF, Osipov R (2000) Plasma kinetics in atmospheric gases, vol. 31. Atomic, Optical and Plasma Physics Series, Springer, Berlin
4. Capitelli M, Colonna G, Gorse C, D'Angola A (2000) Eur Phys J D At Mol Opt Plasma Phys 11:279
5. D'Angola A, Colonna G, Gorse C, Capitelli M (2008) Eur Phys J D 46:129
6. Laricchiuta A, Bruno D, Capitelli M, Catalfamo C, Celiberto R, Colonna G, Diomede P, Giordano D, Gorse C, Longo S, Pagano D, Pirani F (2009) Eur Phys J D 54(3):607
7. Catalfamo C, Bruno D, Colonna G, Laricchiuta A, Capitelli M (2009) Eur Phys J D 54(3):613
8. Bruno D, Catalfamo C, Capitelli M, Colonna G, De Pascale O, Diomede P, Gorse C, Laricchiuta A, Longo S, Giordano D, Pirani F (2010) Phys Plasmas 17(11):112315
9. Capitelli M, Colonna G, Giordano D, Marraffa L, Casavola A, Minelli P, Pagano D, Pietanza L, Taccogna F (2005) J Spacecr Rockets 42(3):980
10. Pagano D, Casavola A, Pietanza LD, Colonna G, Giordano D, Capitelli M (2008) J Thermophys Heat Transf 22(3):8
11. Capitelli M, Colonna G, Gorse C, Minelli P, Pagano D, Giordano D (2002) J Thermophys Heat Transf 16(3):469
12. Giordano D, Capitelli M (1995) J Thermophys Heat Transf 9(4):803
13. Giordano D, Capitelli M (2002) Phys Rev E Stat Nonlin Soft Matter Phys 65(1):016401/1
14. Capitelli M, Armenise I, Bruno D, Cacciatore M, Celiberto R, Colonna G, De Pascale O, Diomede P, Esposito F, Gorse C, Hassouni K, Laricchiuta A, Longo S, Pagano D, Pietanza D, Rutigliano M (2007) Plasma Sources Sci Technol 16(1):S30

15. Capitelli M, Colonna G, D'Angola A (2011) Fundamental aspects of plasma chemical physics: thermodynamics, vol 66 (Springer Series on Atomic, Optical, and Plasma Physics)
16. Colonna G, Capitelli M (2009) Spectrochim Acta Part B At Spectrosc 64(9):863
17. D'Ammando G, Colonna G, Pietanza LD, Capitelli M (2010) Spectrochim Acta Part B At Spectrosc 65:603
18. Capitelli M, Celiberto R, Gorse C, Laricchiuta C, Pagano D, Traversa P (2004) Phys Rev E 69(2):026412
19. Bruno D, Capitelli M, Catalfamo C, Laricchiuta A (2008) Phys Plasmas 15:112306
20. Eletskii AV, Capitelli M, Celiberto R, Laricchiuta A (2004) Phys Rev A 69(4):042718
21. Kosarim A, Smirnov B, Capitelli M, Laricchiuta A (2006) Int J Mass Spectrom 253:22
22. Laricchiuta A, Bruno D, Capitelli M, Celiberto R, Gorse C, Pintus G (2008) Chem Phys 344(1–2):13
23. Laricchiuta A, Pirani F, Colonna G, Bruno D, Gorse C, Celiberto R, Capitelli M (2009) J Phys Chem A 113(52):15250
24. Napartovich AP (2001) Plasmas Polym 6:1
25. Gordiets B, Pinheiro M, Tatarova E, Dias FM, Ferreira CM, Ricard A (2000) Plasma Sources Sci Technol 9(3):295
26. Ionin AA, Klimachev YM, Kotkov AA, Kochetov IV, Napartovich AP, Seleznev LV, Sinitsyn DV, Hager GD (2003) J Phys D Appl Phys 36(8):982
27. Capitelli M, Celiberto R, Colonna G, D'Ammando G, De Pascale O, Diomede P, Esposito F, Gorse C, Laricchiuta A, Longo S, Pietanza L (2010) J Phys B 43(14):144025
28. Colonna G, Capitelli M (1996) J Thermophys Heat Transf 10(3):406
29. Colonna G, Capitelli M (2001) J Phys D Appl Phys 34(12):1812
30. Colonna G, Tuttafesta M, Capitelli M, Giordano D (1999) J Thermophys Heat Transf 13(3):372
31. Colonna G, Pietanza L, Capitelli M (2008) J Thermophys Heat Transf 22(3):399
32. Colonna G, Armenise I, Bruno D, Capitelli M (2006) J Thermophys Heat Transf 20(3):477
33. Capitelli M, Celiberto R, Colonna G, D'Ammando G, De Pascale O, Diomede P, Esposito F, Gorse C, Laricchiuta C, Longo S, Pietanza LD, Taccogna F (2011) Plasma Phys Control Fusion 53(12):124007
34. Loureiro J, Guerra V, Sa PA, Pintassilgo CD, Lino da Silva M (2011) Plasma Sources Sci Technol 20(2):024007
35. Guerra V, Kutasi K, Lino da Silva M, Sa PA, Loureiro J (2010) High Temp Mater Process 14(1–2):141
36. http://users.ba.cnr.it//imip/cscpal38/phys4entry/
37. Esposito F, Capitelli M (2006) Chem Phys Lett 418:581
38. Esposito F, Armenise I, Capitelli M (2006) Chem Phys 331:1
39. Laporta V, Celiberto R (2011). In preparation
40. Laganà A, Ochoa De Aspuru G, Garcia E (1996) Dipartimento di Chimica, Università di Perugia, Perugia, Italy
41. Armenise I, Capitelli M, Colonna G, Gorse C (1996) J Thermophys Heat Transf 10:397
42. Huo WM, Gibson TL, Lima MAP, McKoy V (1987) Phys Rev A 36(4):1632
43. Morgan LA (1986) J Phys B At Mol Phys 19(11):L439
44. Allan M (1985) J Phys B At Mol Opt Phys 18(22):4511
45. Chandra N, Temkin A (1976) NASA Technical Note TN D-8347:69
46. Cacciatore M, Rutigliano M (2009) Plasma Sources Sci Technol 18(2):023002
47. Rutigliano M, Pieretti A, Cacciatore M, Sanna N, Barone V (2006) Surf Sci 600:4239
48. Capitelli M, Bruno D, Colonna G, Catalfamo C, Laricchiuta A (2009) J Phys D 42:194005
49. Bruno D, Capitelli M, Catalfamo C, Laricchiuta A (2007) Phys Plasmas 14:072308
50. Bruno D, Laricchiuta A, Capitelli M, Catalfamo C (2007) Phys Plasmas 14:022303
51. Capitelli M, Celiberto R, Gorse C, Laricchiuta A, Minelli P, Pagano D (2002) Phys Rev E 66(1):016403
52. Capitelli M, Laricchiuta A, Pagano D, Traversa P (2003) Chem Phys Lett 379(5–6):490
53. Singh G, Sharma R, Singh K (2008) J Phys D 41:225203
54. Kosarim A, Smirnov B, Capitelli M, Celiberto R, Laricchiuta A (2006). Phys Rev A 74(6):062707
55. Smirnov BM (2001) Phys Usp 44(3):221
56. Nikitin EE, Smirnov BM (1978) Sov Phys Usp 21(2):95
57. Capitelli M, Colonna G, De Pascale O, Gorse C, Hassouni K, Longo S (2009) Plasma Sources Sci Technol 18(1):014014
58. Longo S, Diomede P (2009) Plasma Process Polym 6:370
59. Longo S, Capitelli M, Diomede P (2004) Lect Notes Comput Sci 3039:580
60. Colonna G, Capitelli M (2008) J Thermophys Heat Transf 22(3):414

61. Colonna G, Capitelli M (2005) In: Capitelli M (ed) AIP conference proceedings of the 24th international symposium on rarefied gas dynamics, vol 762. American Institute of Physics, New York, pp 1295–1300
62. Colonna G, Capitelli M (2001) J Thermophys Heat Transf 15:308
63. Colonna G, Capitelli M (2001) J Phys D Appl Phys 34:1812
64. Capitelli M, Celiberto R, Esposito F, Laricchiuta A (2009) Plasma Process Polym 6:279
65. Schulz GJ (1973) Rev Mod Phys 45(3):423
66. Schulz GJ (1962) Phys Rev 125(1):229
67. Schulz GJ (1964) Phys Rev 135(4A):A988
68. Dubé L, Herzenberg A (1979) Phys Rev A 20(1):194
69. Hazi AU, Rescigno TN, Kurilla M (1981) Phys Rev A 23(3):1089
70. Schneider BI, Le Dourneuf M, Lan VK (1979) Phys Rev Lett 43(26):1926
71. Berman M, Estrada H, Cederbaum LS, Domcke W (1983) Phys Rev A 28(3):1363
72. Mihajlov AA, Stojanovic VD, Petrovic ZL (1999) J Phys D Appl Phys 32(20):2620
73. Bardsley JN, Wadehra JM (1979) Phys Rev A 20(4):1398
74. Capitelli M, Molinari E (1980) Top Curr Phys 90:59
75. Petrović Z, Suvakov M, Nikitović Z, Dujko S, Sasić O, Jovanović J, Malović G, Stojanović V (2007) Plasma Sources Sci Technol 16(1):S1
76. Petrović Z, Dujko S, Marić D, Malović G, Nikitović Z, Sasić O, Jovanović J, Stojanović V, Radmilović-Radenović M (2009) J Phys D Appl Phys 42(19):194002
77. Huo WM, McKoy V, Lima MAP, Gibson TL (1986) Thermo-physical aspects of reentry flows. In: Moss JN, Scott CD (eds) Progress in astronautics and aeronautics series, vol. 103. AIAA, pp 103–423. ISBN-13: 978-0-930403-10-2
78. Laganà A, Garcia E, Ciccarelli L (1987) J Phys Chem 91(2):312
79. Laganà A, Garcia E (1994) J Phys Chem 98(2):502
80. Garcia E, Laganà A (1997) J Phys Chem A 101(26):4734
81. Garcia E, Saracibar A, Laganà A, Skouteris D (2007) J Phys Chem A 111(41):10362
82. Kustova EV, Nagnibeda EA, Alexandrova TY, Chikhaoui A (2003) Chem Phys Lett 377(5–6):663
83. Orsini A, Rini P, Taviani V, Fletcher D, Kustova E, Nagnibeda E (2008) J Thermophys Heat Transf 22(3):390
84. Esposito F, Capitelli M (1999) Chem Phys 302(1–2):49
85. Petrović ZL, Marković VL, Pejović M, Gocić S (2001) J Phys D 34(12):1756
86. Foissac C, Campargue A, Kachanov A, Supiot P, Weirauch G, Sadeghi N (2000) J Phys D Appl Phys 33(19):2434
87. Colonna G, Pietanza L, Capitelli M (2008) J Thermophys Heat Transf 22(3):399
88. Gorse C, Fitting relation based on SSH theory (private communication)
89. Capitelli M, Gorse C, Billing GD (1980) Chem Phys 52(3):299
90. Billing GD, Fisher ER (1979) Chem Phys 43(3):395
91. Capitelli M (1986) Nonequilibrium vibrational kinetics, vol 39. Springer Series Topics in Current Physics
92. Gorse C, Cacciatore M, Capitelli M, De Benedictis S, Dilecce G (1988) Chem Phys 119:63
93. Gorse C, Capitelli M (1987) J Appl Phys 62:4072
94. Dyatko NA, Capitelli M, Longo S, Napartovich AP (1998) Plasma Phys Rep 24:691
95. Dyatko NA, Napartovich AP, Sakadzic S, Petrović Z, Raspopović Z (2000) J Phys D Appl Phys 33(4):375
96. Dyatko NA, Loffhagen D, Napartovich AP, Winkler R (2001) Plasma Chem Plasma Process 21:421
97. Capitelli M, Celiberto R (1998) In: Becker KH (ed) Novel aspects of electron-molecule collisions. World Scientific Publishing, Singapore, p 283
98. Robson RE, White RD, Petrović ZL (2005) Rev Mod Phys 77:1303
99. Galvão BRL, Varandas AJC (2009) J Phys Chem A 113:14424
100. Jaffe R, Schwenke DW, Chaban G (2009) AIAA paper, AIAA 2009–1569
101. Schwenke DW, von Karman Institute Lecture Series (2010)